# 906. A robust scheme for the identification of centerlines of moiré fringes from optical experimental images

**Paulius Palevičius[1], Antanas Sudintas[2], Algimantas Fedaravičius[3], Jūratė Ragulskienė[4]**
[1, 4]Research Group for Mathematical and Numerical Analysis of Dynamical Systems
Kaunas University of Technology, Lithuania
[2]Department of Heat and Nuclear Engineering, Kaunas University of Technology, Lithuania
[3]Institute of Defence Technologies, Kaunas University of Technology, Lithuania
**E-mail:** [1]*paulius.palevicius@ktu.lt*, [2]*antanas.sudintas@ktu.lt*,
[3]*algimantas.fedaravicius@ktu.lt*, [4]*jurate.ragulskiene@ktu.lt*

*(Received 20 October 2012; accepted 4 December 2012)*

**Abstract.** A robust scheme for the identification of centerlines of moiré fringes from optical experimental images is proposed in this paper. The proposed computational algorithm comprises three basic steps: the thresholding of the experimental image, thinning of the projected grating based on morphological and mid-point detection rules and, finally, the reconstruction of the map of continuous curves from the binary matrix of pixels representing fringe centerlines. The first steps can be considered as adaptations of standard image processing techniques, while the identification and the reconstruction of continuous curves is the original contribution specifically developed for optical projection moiré images. The functionality of such an approach is demonstrated for a demanding optical experimental image.

**Keywords:** moiré fringes, centerline identification, pattern detection.

## Introduction

Advanced strain measurement and control tools (including geometric moiré techniques) are regarded as primary technology drivers in such industries as MEMS (micro-electro-mechanical systems) fabrication and high-precision machine tools manufacturing [1], [2], [3]. Accurate interpretation of experimental measurement results is one of the crucial factors enabling the minimization of the general uncertainty budget. Particularly that is important in projection moiré application where it is common that poor illumination conditions, non-uniform distribution of moiré fringes in the observation area, complex surfaces of the investigated systems and noisy background does not allow a reliable interpretation of the optical measurement results.

The interpretation of the projected array of moiré grating lines can be separated into two basic blocks – the identification of centerlines of the projected fringes and the reconstruction of maps of the measured physical quantity (strain, amplitude of deformation, etc.). And while the second task can be taken as an almost standard feature of any contour-based 3D plotting software package, the computational derivation of the contour maps is still very much dependent on particular implementations. Interpretation of projected moiré fringes is not a straightforward task even for a static double-exposure problem.

As mentioned previously, applicability of the projection moiré for more complex structures in more demanding environments requires reliable computational tools for the interpretation of experimental images. The reconstruction of the 2D map of fringe centerlines is one of the main factors ensuring the accuracy of the interpretation of optical measurement results. The main objective of this paper is to propose a general scheme for the construction of the centerline contour map from an experimental optical projection moiré image. The proposed computational technique comprises three main steps:

1. The thresholding of the experimental image.
2. Thinning of the projected grating based on morphological and mid-point detection method.

3. The reconstruction of the map of continuous curves from the binary matrix of pixels representing fringe centerlines.

## 1. The description of the experimental setup

The general view of the optical experimental setup comprising a PC, digital camera, projector, and the test object is shown in Fig. 1 (a). It can be noted that this instrument has been used for measuring paper vibrations in a printing machine where paper band rolls at relatively high speeds [4]. A digital image of an array of dark and white stripes is projected onto the surface of a printed circuit board (PCB); the angle of the incident light is 20 degrees what ensures a satisfactory identification of the surface deformation and prevents excessive formation of shadows [5].

The main objective of this paper is the development of a reliable algorithm for the reconstruction of 2D map of centerlines of projected fringes. We do concentrate on the computational aspects of the algorithm in the next sections and use the experimental image in Fig. 1 (b) as the test for the proposed approach.

a) 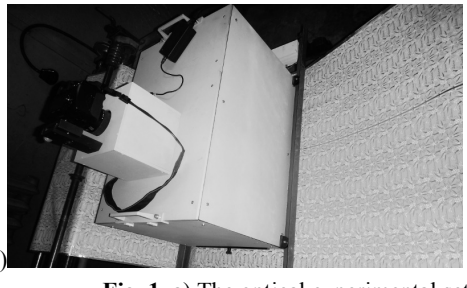 b) 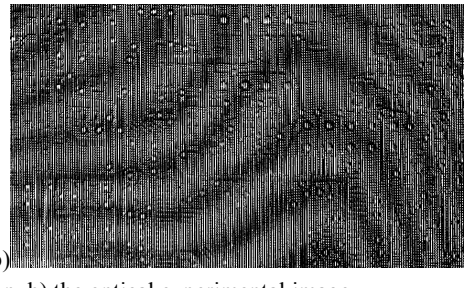

**Fig. 1.** a) The optical experimental setup, b) the optical experimental image

## 2. Thresholding operation for the optical moiré images

The first step towards the identification of centerlines is the construction of a binary representation of the optical experimental grayscale image. The quality of the resulting binary image is crucial for the remaining steps. Various thresholding techniques can be exploited for the construction of the binary representation of the original experimental image [6] (though not all of them may produce a desired result). Thresholding may be viewed as an operation that involves tests against a function $T$ of the form:

$$T = [x, y, f(x, y), p(x, y)], \tag{1}$$

where $f(x, y)$ is the gray level of point $(x, y)$ (the original experimental image) and $p(x, y)$ denotes some local property of this point [7]. A thresholded image $g(x, y)$ is defined as:

$$g(x, y) = \begin{cases} 1, & f(x, y) < T, \\ 0, & f(x, y) \geq T. \end{cases} \tag{2}$$

The threshold is called global in case when $T$ depends only on $f(x, y)$ and the threshold is called local [7] if $T$ depends on both $f(x, y)$ and $p(x, y)$.

It is clear that straightforward application of global thresholding methods (like histogram shape-based methods) to the test image cannot produce acceptable results due to the non-

uniformity of lighting Fig. 2 (a); even though global methods are fast and reliable with images having uniform lighting [8].

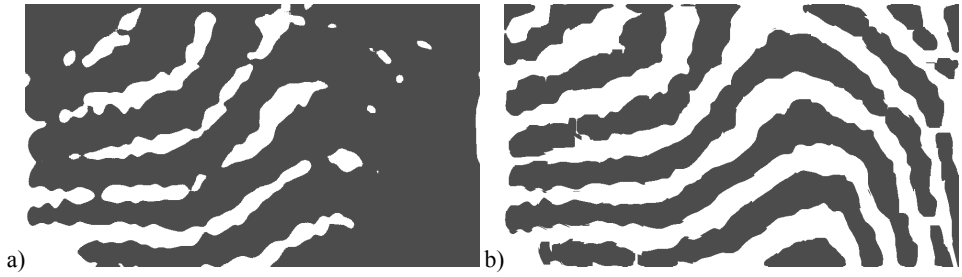


**Fig. 2.** a) Result of global thresholding,
b) binary representation of image when using local thresholding method

Local thresholding based on average gray value of neighboring pixels surrounding the current pixel ($x$, $y$) are to be used in order to produce the binary image Fig. 2 (b).

The structure of the original optical image suggests that initial smoothing before the thresholding procedure may help to gain better representation of fringes in the thresholded image.

## 3. Thinning of the projected grating based on mid-point detection and rules morphological

Two alternative techniques for the thinning of the projected grating from the thresholded experimental image are investigated in this section. Both techniques can be also considered as standard image processing techniques – we just adapt both methods for optimal processing of projected moiré images.

### 3.1. The mid-point detection method

The method is based on the algorithm proposed in [9] and later investigated in [8]. It uses vertical and horizontal scan lines to determine mid-points of each dark and bright fringe. The detailed description of this method is given in [8]; it is based on global thresholding and row-column-wise scanning.

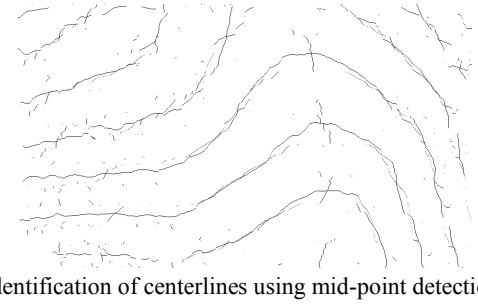

**Fig. 3.** Identification of centerlines using mid-point detection method

Nevertheless, direct application of the algorithm proposed in [8] would produce poor results due to non-uniform lightning conditions in the initial experimental image. And though local thresholding and image smoothing operations can improve the functionality of the mid-point detection method, the described row and column scans still produce an unsatisfactory image (as

shown in Fig. 3) due to a large number of fractures in the pattern of centerlines and loose spurs in areas between centerlines.

### 3.2. Mathematical morphological operations

Mathematical morphology [10] is a tool for extracting image components that are useful in representation and description of regions or shapes such as boundaries of a region, skeletons or other patterns. In this paper we will use the thinning operation [7] based on the hit-or-miss algorithm since simple erosion operation would destruct smaller parts of moiré fringes in the thresholded image. The structuring elements $B_i$ will be used for hit-or-miss operation.

**Table 1.** Structuring elements $B_1$ and $B_2$ used for thinning

| | | |
|---|---|---|
| 0 | 0 | 0 |
| | 1 | |
| 1 | 1 | 1 |

| | | |
|---|---|---|
| | 0 | 0 |
| 1 | 1 | 0 |
| 1 | 1 | 0 |

The execution of the thinning process produces undesired parasitic components (spurs) around actual centerlines of moiré fringes Fig. 4 (a). These spurs are caused during erosion by non-uniformities in objects and may be removed by performing the pruning operation [7].

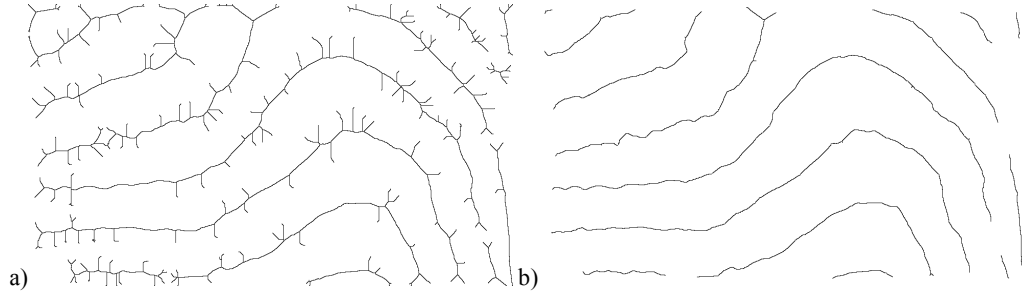


**Fig. 4.** a) Result of thinning operation against thresholded image,
b) the final result of identification of centerlines using mathematical morphological operations

A smooth and noise-free pattern of centerlines is produced in the result of the described digital image processing operations Fig. 4 (b). Unfortunately, a number of intermittent broken centerlines can still be visible. Some of these defects are caused by optical defects in the original image. Appropriate identification and joining of broken centerlines could considerably improve the quality of interpretation of the optical experimental image and is the main contribution of this paper.

## 4. Identification of individual centerlines

So far fringe thinning operations resulted into a matrix of black and white pixels. The joining of broken centerlines requires identification of continuous intervals of curves in produced digital image. The main objective of this section is to develop a reliable method for grouping sets of adjacent pixels into curves and filling possible fractures inside separate curves. The proposed method can be divided into the following steps:

- Division of image into grid cells;
- Derivation of approximate line equation in each cell containing black pixels;
- Grouping contacting cells into curves;
- Identification and joining of curves with fractures.

### 4.1. Division of image into grid cells

In general, the selection of the size of the grid cell $w_g$ is an empirical procedure, but it should be related to the density of moiré fringes in the original optical image. The main requirement from the point of reliable functionality of the proposed algorithm is that there should be only one centerline passing through each grid cell. On the other hand a larger cell size increases the performance of the proposed method.

### 4.2. Derivation of approximate line equation in each cell containing black pixels

The algorithm is started by sweeping cells of the thinned image (from left to right and from top to bottom) searching for cells containing black pixels. In case the current cell contains black pixels we try to identify the following parameters of the line crossing that cell: the slope, the intercept, the angle and the mid-point of the line (it is assumed that the cell size is small enough to represent a curve as a line segment inside the cell). Several alternative options for the construction of a line in a cell exist:

1. Identification of black pixels on the boundaries of the current cell and the construction of a line running through these pixels.
2. Construction of the linear statistical regression line through the array of black pixels in the current cell.
3. Exploiting Hough (Radon) digital image transforms for the identification of a line in the current cell.

The first option is the fastest solution from all three, but is not viable because the thinned curves may break near the boundary of the current cell. Moreover, this method is not resistant to the additive noise what could significantly distort the resulting image.

The method based on the linear statistical regression would cope with the additive noise well, but problems would occur when vertical lines should be reconstructed in the current cell.

Radon [11] or Hough [12] transforms are probably the most reliable solution for robust identification of a line in a cell. Both transforms can be effectively used for the detection of simple shapes such as lines, circles, ellipses by making a transformation from the image space to the parameter space. To gain better performance a variant of Hough transform - Randomized Hough transform (RHT) [13] was selected and then applied to every cell of the thinned image.

A new matrix of vectors comprising basic line parameters (the angle $\theta$ and the location of the line mid-point $x$ and $y$ in each grid cell) is constructed from the output data of the RHT:

$$G = \left\{ \left( \theta_{i,j}, x_{i,j}, y_{i,j} \right) \mid i \in \left[ 1, m_g \right], j \in \left[ 1, n_g \right] \right\}, \tag{5}$$

where $m_g \times n_g$ is the number of grid cells in the vertical and the horizontal directions. It is possible that more than one line can be discovered in a cell due to noise or spurs; thus the longest line interval is identified as the part of the reconstructed curve.

### 4.3. Grouping contacting cells into curves

The proposed method for grouping contacting cells into curves is given below:

(i) Append a single layer of empty grid cells around the grid matrix $G$.

(ii) Proceed with cells from left to right and from top to bottom starting at cell $G_{1,1}$.

(iii) Check if there are cells with an assigned line in the immediate surroundings of $G_{i,j}$ (Fig. 5 (a)).

(iv) Select a nearest cell with the assigned line $G_{k,1}$ to the current cell $G_{i,j}$ and assign $G_{k,1}$ to the set of cells belonging to the same curve $C_i$ (Fig. 9 (b)). Remove cell $G_{i,j}$ from the $G$ matrix (Fig. 5 (b)).

(v) Repeat step (iii - iv) with cells $G_{k,1}$ until $G_{k,1}$ has no surrounding cells with assigned lines.

(vi) Return to cell $G_{i,j}$ and continue with the next cell in a row (column); go to step (iii).

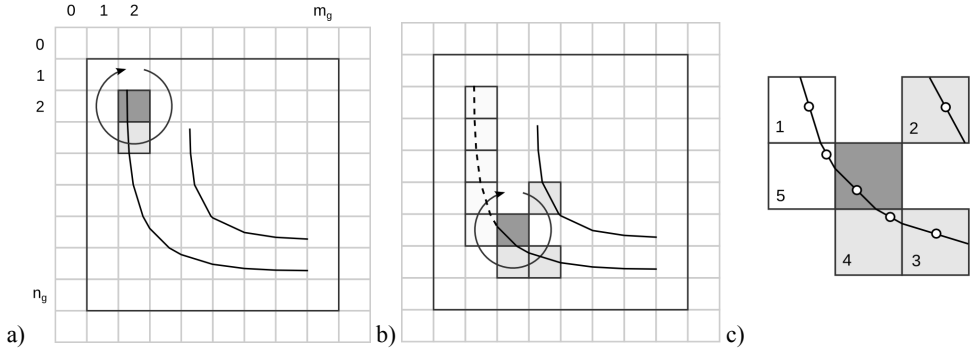


**Fig. 5.** a) Scanning for cells with assigned lines around the current cell (marked as the dark gray cell). b) A schematic diagram illustrating the selection of the next grid cell. First image shows the current cell in dark gray and unprocessed cells (with the assigned line) in the vicinity of the current cell in light gray. The thick light gray line denotes the set of cells assigned to the current curve. c) Illustrates the selection of correct nearest neighbors – cell 4 is selected instead of cell 3 or cell 2 (it belongs to the other curve); empty circles denote line centers inside appropriate cells

### 4.4. Identification and joining of curves with fractures

Some curves may have fractures larger than one cell due to defects in the initial image or loss of information during the previously described steps. An adaptive method for the identification and joining of curves with fractures is proposed in this section.

A set of curves is already identified (each curve is associated to a set of cells). Thus it is possible to define various criteria that could be used to decide if two separate curves could be joined. The first criterion that we define is the distance between the edge cells of the curve:

$$d_{i,j} = \sqrt{\left(x_i - x_j\right)^2 + \left(y_i - y_j\right)^2}, \tag{6}$$

where ($x_i$, $y_i$) and ($x_j$, $y_j$) are all possible pairs of the center points of the edge cells of the identified curves.

The other criterion could be the orientation between edge cells of curves $\left|\theta_i - \theta_j\right|$. Anyway, a number of computational experiments have shown that there could be situations where that criterion does not work as expected. Thus an alternative criterion reads Fig. 6:

$$a_{i,j,1} = \left|\theta_i - \theta_{i,j}\right| \text{ and } a_{i,j,2} = \left|\theta_j - \theta_{i,j}\right|, \tag{7}$$

where $\theta_{i,j}$ is the angle of line running through points ($x_i$, $y_i$) and ($x_j$, $y_j$) and the $x$-axis.

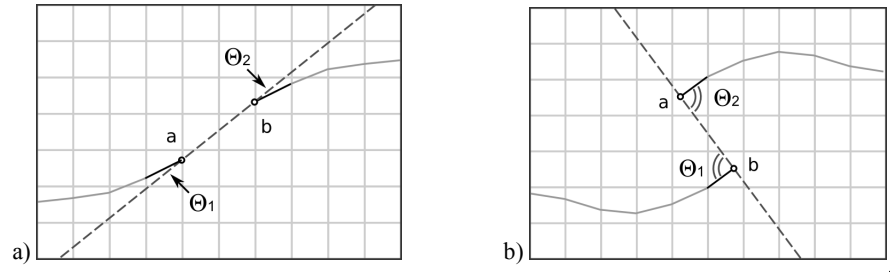


**Fig. 6.** a) A schematic diagram illustrating a favorable connection between two curves; the $\left|\theta_i - \theta_j\right|$ criterion would be sufficient for the detection of similar angles between lines in the edge cells. b) A schematic diagram illustrating an unfavorable connection between two curves; the $\left|\theta_i - \theta_j\right|$ criterion would suggest a connection while the alternative criterion eliminates a possible connection between the edge cells

Maximum allowed values for defined criteria should be selected depending on the complexity initial image. In our case we constrained $d_{i,j}$ to the double width of a cell and the values of parameters $a_{i,j,1}$ and $a_{i,j,2}$ are limited to 30 degrees.

We also define the applicable value of the parameter $J_{i,j}$ which is used when there are more than one curve holding against defined criterion constraints:

$$J_{i,j} = \frac{1}{\alpha d_{i,j} + \beta\left(a_{i,j,1} + a_{i,j,2}\right)}, \tag{8}$$

where $\alpha$ and $\beta$ are weights which allow to emphasize the importance of the distance between the edges or the variation of angles at the edges. The defined curve joining criterions are incorporated into the proposed algorithm for curve joining:

(i) Select a curve $C_i$ from the set $C$.

(ii) Compute criteria $d_{i,j}$, $a_{i,j,1}$, $a_{i,j,2}$ between curves $C_i$ and $C_j$; $i \neq j$ for all available edges.

(iii) Merge all cells of the curve $C_j$ with $C_i$ for such $i$ and $j$ minimizing the value of $J_{i,j}$ on the corresponding edges. Remove $C_j$ from the set $C$ and repeat steps (ii-iii) until there are no more favorable connections.

(iv) Proceed with the curve $C_i$ and repeat steps (i-iii).

The result of this procedure can be seen in Fig. 7 (compare the reconstructed pattern to Fig. 4 (b)). It can be noted that the produced pattern of centerlines is produced from a noisy low quality experimental image with uneven illumination and highly expressed background.

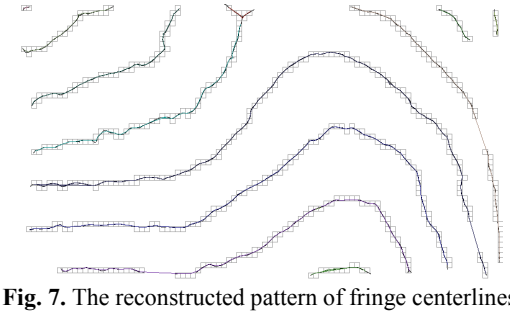

**Fig. 7.** The reconstructed pattern of fringe centerlines

## Conclusions

A unified scheme for the identification of centerlines of moiré fringes from optical experimental images is presented in this paper. This scheme is partly based on standard algorithms of digital image processing. On the other hand, specific algorithmic implementation and original line tracing methods make this scheme robust to noise and various distortions in the original optical image.

The main objective of this paper is to propose a reliable scheme for the construction of 2D map of fringe centerlines, since that in the main source of errors and uncertainties in the quantitative interpretation of fringe based optical moiré images. In other words, we do not consider the reconstruction of maps of the measured physical quantity (strain, amplitude of deformation, etc.) what can be effectively done by using standard contour-based 3D plotting algorithms.

Robust identification of fringe centerlines is particularly important in shadow and projection moiré applications where it is common that poor illumination conditions, non-uniform distribution of moiré fringes in the observation area, complex surfaces of the investigated systems and noisy backgrounds do not allow a reliable interpretation of optical measurement results. Reliable identification of fringe centerlines is especially important in optical MEMS analysis what is a definite object of future research.

## References

**[1]** **H. Shang, H. Xie, X. Wang, S. Jiang, F. Dai, W. Wang, et al.** Thermal properties measurement of micro-electromechanical system sensors by digital moiré method. Strain, Vol. 41, 2005, p. 157–162.

**[2]** **B. Han** Recent advancements of moiré and microscopic moiré interferometry for thermal deformation analyses of microelectronics devices. Experimental Mechanics, Vol. 38, 1998, p. 278–288.

**[3]** **C. A. Sciammarella, F. M. Sciammarella, T. Kim** Strain measurements in the nanometer range in a particulate composite using computer-aided moiré. Experimental Mechanics, Vol. 43, 2003, p. 341–347.

**[4]** **M. Ragulskis, A. Aleksa, R. Maskeliūnas** Contrast enhancement of time-averaged fringes based on moving average mapping functions. Optics and Lasers in Engineering, Vol. 47, 2009, p. 768–773.

**[5]** **M. Ragulskis, Z. Navickas** Interpretation of fringes produced by time-averaged projection moiré. Strain, Vol. 47, 2011, p. 357–370.

**[6]** **M. Sezgin, B. Sankur** Survey over image thresholding techniques and quantitative performance evaluation. Journal of Electronic Imaging, Vol. 13, 2000, p. 146.

**[7]** **R. Gonzalez** Digital Image Processing. Second Ed., Pearson Education, Delhi, 2002.

**[8]** **A. Anand** Tracing of interference fringes using average gray value and simultaneous row and column scan. Optics & Laser Technology, Vol. 35, 2003, p. 73–79.

**[9]** **V. Parthiban** Interactive fringe processing algorithm for interferogram analysis. Optics and Lasers in Engineering, Vol. 11, 1989, p. 103–113.

**[10]** **J. P. Serra** Image Analysis and Mathematical Morphology. Academic Press, London, New York, 1982.

**[11]** **J. Radon** Über die bestimmung von funktionen durch ihre integralwerte längs gewisser mannigfaltigkeiten. Akad. Wiss., Vol. 69, 1917, p. 262–277.

**[12]** **R. O. Duda, P. E. Hart** Use of the Hough transformation to detect lines and curves in pictures. Communications of the ACM, Vol. 15, 1972, p. 11–15.

**[13]** **L. Xu, E. Oja, P. Kultanen** A new curve detection method: Randomized Hough Transform (RHT). Pattern Recognition Letters, Vol. 11, 1990, p. 331–338.